J. Mech. Phys. Solids 206 (2026) 106388

Contents lists available at ScienceDirect

Journal of the Mechanics and Physics of Solids

journal homepage: www.elsevier.com/locate/jmps

Adhesive contact of elastic spherical shells: Non-monotonic thickness dependence of pull-off force

Shi-Wen Chen [a], Gang-Feng Wang [a], Michele Ciavarella [b,c,*]

[a] Xi'an Jiaotong University, Department of Engineering Mechanics, SVL and MMML, 710049 Xi'an, PR China
[b] Politecnico di BARI, DMMM department, Viale Gentile 182, 70126 Bari, Italy
[c] Hamburg University of Technology, Department of Mechanical Engineering, Am Schwarzenberg-Campus 1, 21073 Hamburg, Germany

ARTICLE INFO

Keywords:
Elastic shell
Adhesion
Contact mechanics

ABSTRACT

The adhesive contact of spherical shells is a critical problem across multiple length scales. In this study, we investigate the adhesive contact between an elastic spherical shell and a rigid plane. Two independent approaches are employed: the JKR theory from an energy perspective, and a simulation-based method incorporating a traction-separation law. Our results reveal a non-monotonic relationship between pull-off force and shell thickness. Specifically, for relatively thick shells, the pull-off force decreases with decreasing thickness; however, below a critical thickness, this trend reverses, and the pull-off force begins to increase. Furthermore, we explore the underlying mechanisms responsible for this behavior and examine the influence of adhesion parameters on the overall response.

1. Introduction

Spherical shells are structures of significant research and application value across a wide range of scales, such as viral capsids (Michel et al., 2006), nano- or micro-capsules (Elsner et al., 2004; Fery and Weinkamer, 2007; Delcea et al., 2011), tactile sensors (Youssefian et al., 2014), and soft grippers (Zhao et al., 2025). In these examples, surface adhesion significantly affects the functional and mechanical responses of their structures. Nonetheless, the adhesive contact of spherical shells remains insufficiently understood and therefore warrants a renewed investigation.

Adhesive contact has been studied for over half a century, with early research primarily focusing on elastic solid spheres. Johnson, Kendall, and Roberts (JKR) presented one of the most influential models (Johnson et al., 1971), in which the adhesive contact of an elastic sphere is described as a superposition of non-adhesive (Hertz theory, see for example (Johnson, 1985)) and flat-punch solutions, with the equilibrium state obtained by minimizing the total energy. Derjaguin, Muller, and Toporov (DMT) proposed another classical model (Derjaguin et al., 1975), assuming that adhesion acts exclusively outside the contact area, effectively treating the sphere's response as a Hertzian contact with an added external force. However, the JKR and DMT models predict different pull-off forces. This discrepancy was later explained by Tabor (1977), who introduced a dimensionless parameter, now known as the Tabor parameter, defined as the ratio between the height of the "neck" around the contact zone and the range of interfacial interaction. The JKR and DMT models represent two limiting cases of adhesive contact: the JKR model applies when the interaction range is much shorter than the neck height, corresponding to a large Tabor parameter, whereas the DMT model is valid when the interaction range is relatively long, corresponding to a small Tabor parameter. To bridge the gap between the JKR and DMT limits, numerous models applicable to finite Tabor parameters have been developed. Notable examples include the model (Muller et al., 1980) employing the

* Corresponding author at: Politecnico di BARI, DMMM department, Viale Gentile 182, 70126 Bari, Italy.
E-mail address: Mciava@poliba.it (M. Ciavarella).

https://doi.org/10.1016/j.jmps.2025.106388
Received 7 May 2025; Received in revised form 25 September 2025; Accepted 30 September 2025
Available online 8 October 2025

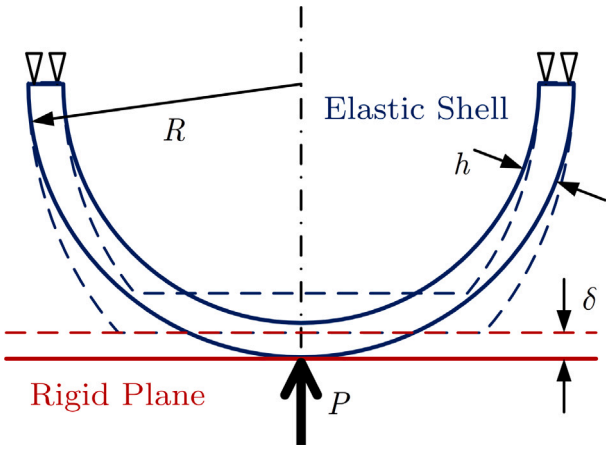

Fig. 1. Schematic for the adhesive contact between a elastic shell and a rigid plane.

Dugdale cohesive zone (Dugdale, 1960) and models that describe interfacial forces using Lennard-Jones potential (Maugis, 1992; J.A., 1997). It should be noted that an adhesion map has been proposed to indicate the applicability of different models (Johnson and Greenwood, 1997).

Based on these foundational models, the study of adhesive contact has been further developed to account for diverse material behaviors—including viscoelasticity (Greenwood and Johnson, 1981; Greenwood, 2010; Ciavarella, 2022) and hyperelasticity (Yang, 2011)—as well as a wide range of geometric configurations, for instance flat-punch (Kendall, 1971), cone (Vallet and Barquins, 2002) and membrane (Yuan et al., 2024; Yu et al., 2024; Zheng and Dai, 2025). In addition, the peeling of thin films is another important problem that has attracted considerable research attention (Rivlin, 1997; Afferrante et al., 2013; Chen and Dai, 2023; Shen et al., 2024).

Although still relatively limited compared to solid spheres, the contact behavior of spherical shells has already been explored in many detailed studies. Pauchard et al. (1997), Pauchard and Rica (1998) were among the first to investigate the adhesionless contact of spherical shells. In their experimental investigation of elastic spherical shells in contact with a rigid plane, Pauchard et al. found that an initially flat contact transitions to a buckled, indented state once the indentation depth approaches about twice the shell thickness. In more detail, as the indentation depth increases, the contact response of a spherical shell can be categorized into several stages: initially a small-deformation regime, followed by a flat-contact phase, then an axisymmetric buckling stage (Sahli et al., 2024), and finally a non-axisymmetric buckling stage (Knoche and Kierfeld, 2014; Vaziri, 2009). Moreover, Tamura et al. (2004), Komura et al. (2005) considered adhesion through Lennard-Jones potential and observed that the contact behavior still followed a sequence of four stages similar to those found in the adhesionless case. It is worth emphasizing that even with adhesion taken into account, they found that the onset of initial buckling still occurred at an indentation depth of approximately twice the shell thickness. Hence, by restricting the indentation depth to less than twice the shell thickness, the analysis can be confined to the pre-buckling regime.

This work is motivated by inconsistencies in the pull-off force reported in previous studies. Shi et al. (2011) presented an analytical result suggesting that the pull-off force increases as the shell thickness decreases; however, their model does not recover the limit for solid spheres, indicating a lack of generality. In contrast, Zhao et al. (2024, 2022) reported that the pull-off force decreases with decreasing shell thickness. Their experimental results, however, revealed a noticeable increase in the pull-off force at very small thicknesses. These discrepancies highlight the need for a more comprehensive understanding of adhesive contact in spherical shells. In this work, we aim to provide results that show clearer agreement with experimental observations.

2. Methodology

Consider an elastic spherical shell in contact with a rigid plane, as shown schematically in Fig. 1. The outer radius is R and the thickness is h. The reduced modulus of the material is $E^* = E/(1-\nu^2)$, where E is the Young's modulus and ν is the Poisson's ratio. The load on the rigid plane is P and the displacement is δ. The work of adhesion $\Delta\gamma$ is defined by $\Delta\gamma = \gamma_1 + \gamma_2 - \gamma_{12}$, where γ_1 and γ_2 are the surface energy density of the two surfaces and γ_{12} is the density of interfacial energy, and the equilibrium distance ϵ is defined as the distance at which the interfacial traction is zero, which typically reflects the characteristic range of the interfacial interaction (Tabor, 1977). When $\epsilon = 0$, it implies that there is no interaction outside the contact zone. In this case, the JKR approach can be employed for analysis from an energy perspective. For a finite ϵ, however, short-range interactions between the surfaces after separation must be taken into account. In this study, both scenarios are considered.

2.1. Dimensional analysis

As a preliminary step toward a comprehensive understanding of the problem, a dimensional analysis is conducted. The problem is characterized by seven variables but only involves two independent dimensions. According to the Buckingham Π theorem (see, for example, Longair (2020)), the system can be described using five dimensionless variables. We consider the load as an output and normalize it as $P/(1.5\pi R\Delta\gamma)$, where $1.5\pi R\Delta\gamma$ is the pull-off force predicted by the JKR theory for solid spheres. The remaining dimensionless variables are chosen such that

$$\frac{P}{1.5\pi R\Delta\gamma} = f\left(\frac{\delta}{R}, \frac{h}{R}, \frac{\Delta\gamma}{E^* R}, \mu\right) \tag{1}$$

Here, μ is the Tabor parameter, defined as (Tabor, 1977):

$$\mu = \left(\frac{R\Delta\gamma^2}{E^{*2}\epsilon^3}\right)^{1/3} \tag{2}$$

The minimum value (note that negative values indicate attractive forces) on the P-δ curve corresponds to the force required to separate the shell from the rigid plane under force-controlled loading. This quantity, known as the pull-off force, is denoted by P_{off} and is given by

$$\frac{P_{\text{off}}}{1.5\pi R\Delta\gamma} = g\left(\frac{h}{R}, \frac{\Delta\gamma}{E^* R}, \mu\right) \tag{3}$$

It should be noted that when $h/R = 1$, the shell becomes a solid sphere. In classical studies of adhesion between solid spheres, including the JKR theory, the DMT theory, and various models for intermediate Tabor parameter, it has been shown that $P_{\text{off}}/(1.5\pi R\Delta\gamma)$ primarily depends on the Tabor parameter μ, indicating that the effect of $\Delta\gamma/(E^* R)$ is negligible. However, in the case of spherical shells, the influence of $\Delta\gamma/(E^* R)$ remains unclear and warrants further investigation.

2.2. The JKR approach

As aforementioned, if the equilibrium distance ϵ is nearly zero, the adhesive contact problem of shell can be considered under the JKR framework. Under the JKR framework, a virtual deformation process is introduced to achieve the actual contact state: First, loading is applied without considering adhesion until a certain contact area is reached. Then, while keeping the contact area unchanged, unloading is performed. The deformation state that minimizes the total energy (the sum of strain energy, surface energy, and external work) corresponds to the deformation state that accounts for adhesion.

In this work, we restrict the actual indentation depth to below twice the shell thickness in order to avoid the onset of buckling in the deformation process (Tamura et al., 2004). Then, to achieve the actual deformation state without buckling, the virtual loading process should ensure that the contacted region does not separate, followed by unloading while keeping the contact area unchanged.

According to previous studies, the JKR solution for linear elastic bodies with a convex interface can be rigorously given based on only the "adhesionless" loading results (Shull, 2002; Ciavarella, 2018). Specifically, the solution is written as (Ciavarella, 2018)

$$P_{\text{Ad}} = P_{\text{N}}(\delta_1) + \left(\frac{\partial P_{\text{N}}}{\partial \delta_{\text{N}}}\right)_{\delta_1} (\delta_{\text{Ad}} - \delta_1) \tag{4}$$

$$\delta_{\text{Ad}} = \delta_1 - \sqrt{2\Delta\gamma \left(\frac{\partial A_{\text{N}}}{\partial \delta_{\text{N}}}\right)_{\delta_1} \Big/ \left(\frac{\partial^2 P_{\text{N}}}{\partial \delta_{\text{N}}^2}\right)_{\delta_1}} \tag{5}$$

Here, P_{Ad} and δ_{Ad} represent the load and displacement considering adhesion, while P_{N}, A_{N} and δ_{N} denote the load, contact area and displacement in the absence of adhesion, under the condition that the contacted region remains intact and does not separate again. In these formulations, since the contact area remains unchanged during the virtual unloading process, the same area A_{N} can be used to represent the adhesive contact.

The results of 'adhesionless' contact under the no-separation condition can be obtained through finite element method (FEM) simulations, with the help of Abaqus Implicit solver. From Eq. (4) and (5), we can see that since the first derivative of the contact area and the first and second derivatives of the load are required, high numerical accuracy is essential. Therefore, significant mesh refinement within the contact region is necessary. The elastic shell is modeled as an axisymmetric model, with an example of the mesh ($h/R = 0.03$) shown in Fig. 2. The shell is divided into 4-node axisymmetric CAX4 elements. For cases with thickness ranging from $h/R = 0.004$ to 0.8, the number of nodes varies from 486136 to 534340, and the number of elements ranges from 482092 to 530140. The element size gradually increases from 1×10^{-3} μm to 0.5 μm along the outer surface of the shell, with the finest mesh concentrated near the lowest point of the shell. At the same time, the displacement loading step is chosen to be sufficiently small, yet still much larger than the mesh size projected onto the loading direction. This ensures that the resulting area–displacement curve is relatively smooth and maintaining the accuracy of the second derivative. In this section, linear elastic material behavior is assumed, and geometric nonlinearity is not considered. In all the simulations, the Young's modulus, the Poisson's ratio and the outer radius are set as $E = 1$ MPa, $\nu = 0.45$ and $R = 100$ μm, respectively. As a reference, Fig. 3 presents several curves of P_N, A_N with respect to δ_N obtained by FEM. By numerically differentiating these data and substituting the results into Eqs. (4) and (5), the adhesive solution in the JKR framework can be derived.

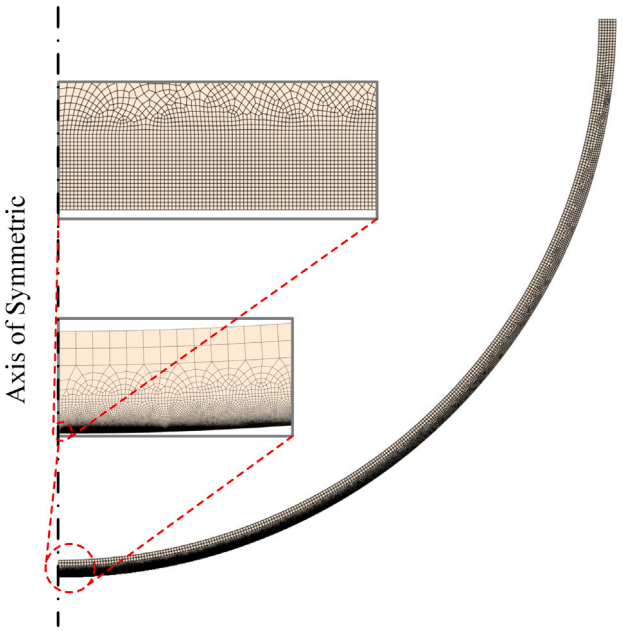

Fig. 2. The axisymmetric FEM model of the elastic spherical shell.

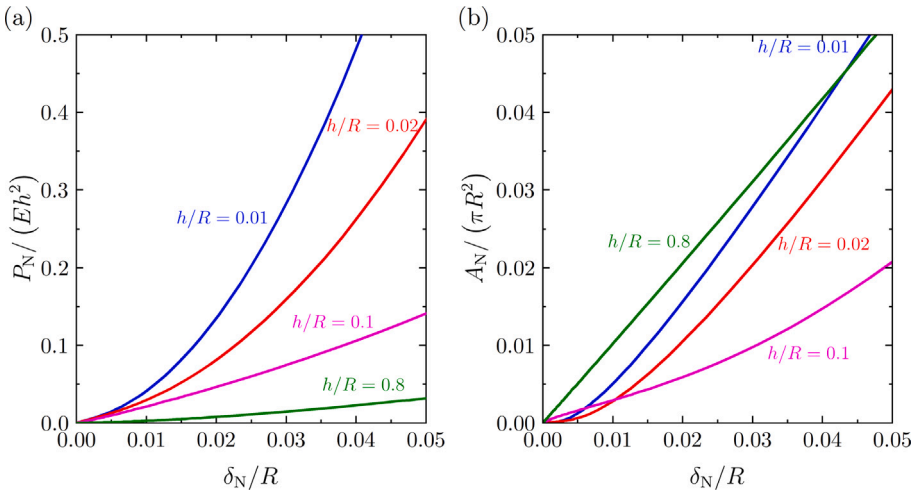

Fig. 3. The 'adhesionless' results under no-separation condition for different thicknesses. (a) $\delta_N - P_N$ curves; and (b) $\delta_N - A_N$ curves.

2.3. Approach to account for interfacial traction law

When the equilibrium separation ε is finite, the interaction between the two surfaces can be described by a traction-separation law, which relates the interfacial traction to the distance between the surfaces. The specific form of the traction law has only a minor effect on the results (Johnson and Greenwood, 1997); the key parameters governing the response are the work of adhesion $\Delta\gamma$ and the equilibrium distance ε. Following many previous works, we adopt a Lennard-Jones-type interaction to model the interface (Kadin et al., 2008; Song and Komvopoulos, 2011), which defines the traction-separation relationship as follows:

$$T(s) = \frac{8\Delta\gamma}{3\varepsilon}\left[\left(\frac{\varepsilon}{s}\right)^3 - \left(\frac{\varepsilon}{s}\right)^9\right] \tag{6}$$

Here, $T(s)$ denotes the interfacial traction (i.e., the attractive force per unit area), and s represents the separation between the two surfaces. The simulations in this section are also conducted utilizing Abaqus Implicit solver. Here, the material is also linear elastic, but geometric nonlinearity is included, which has been shown in a recent study to be the primary source of finite strain effects in contact problems (Mu et al., 2025). Cartesian type connectors are adopted to implement Eq. (6) at the interface. The mesh

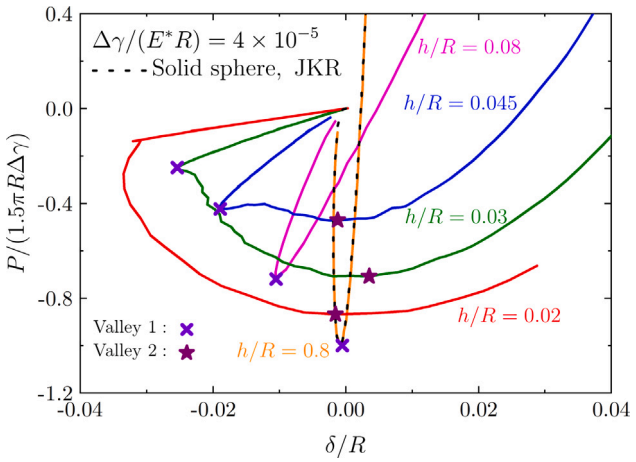

Fig. 4. Load–displacement relationship for different thicknesses at $\frac{\Delta\gamma}{E^*R} = 4 \times 10^{-5}$.

for the shell is similar to that shown in Fig. 2. However, since no differentiation operations are required, a coarser mesh is sufficient to achieve satisfactory numerical accuracy. The number of nodes ranges from 18226 to 71068, and the number of elements from 16326 to 69957, for thickness values ranging from $h/R = 0.006$ to 0.8. The movement of the rigid plane is displacement-controlled.

3. Results in the JKR limit

As an important scenario, we first present the results in the JKR limit. Fig. 4 shows how the load–displacement relationship varies with thickness at $\Delta\gamma/(E^*R) = 4 \times 10^{-5}$. The JKR solution for a solid sphere is also included and agrees well with the result for $h/R = 0.8$, thereby validating our method. The valleys on the curves indicate debonding under force control, where the corresponding load represents the pull-off force. For large thicknesses, only a single valley is observed and is marked as "Valley 1" in Fig. 4, and the associated pull-off force decreases as the thickness is reduced. However, as the thickness is further decreased, a second valley (marked as "Valley 2" in Fig. 4) appears, with its corresponding force increasing and eventually surpassing that of the first valley. Beyond this point, the force associated with the second valley continues to increase, leading to an overall rise in the pull-off force. Notably, the pull-off force reaches its minimum when the forces corresponding to the two valleys become equal.

In Fig. 5, the pull-off force is extracted and presented in a dimensionless form as a function of h/R. From Eq. (3) we know that $\Delta\gamma/(E^*R)$ also has an effect to the pull-off force, so we plotted curves for different $\Delta\gamma/(E^*R)$. Across different parameter values, the pull-off force exhibits a non-monotonic dependence on thickness. This trend arises from the competition between the two valleys, as discussed in the preceding paragraph. The pull-off force exhibits several important limiting cases. Firstly, it is clear that when h/R approaches 1, the pull-off force converges to the value predicted by the JKR theory of solid spheres, which is independent on $\Delta\gamma/(E^*R)$. Secondly, the pull-off force exhibits a minimum value. From Fig. 5, we can observe that the minimum value and its corresponding thickness vary for different $\Delta\gamma/(E^*R)$ values. However, for the range of $\Delta\gamma/(E^*R)$ values we calculated, spanning approximately three orders of magnitude, the ratio of the minimum pull-off force to the JKR result remains greater than 0.4.

The third important limiting case is when the thickness approaches zero. Lower thickness values could not be computed due to numerical precision limitations. However, Fig. 5 clearly shows a decrease in the rate at which the pull-off force increases as the thickness decreases. When $\Delta\gamma/(E^*R) = 1.6 \times 10^{-3}$ and the pull-off force approaches the solid-sphere limit, the rate of increase becomes nearly zero. For $\Delta\gamma/(E^*R) = 4 \times 10^{-4}$ and 4×10^{-5}, the ratio between the pull-off force and the solid-sphere result becomes similarly close for $h/R = 0.006$, yet the rate of increase remains higher for $\Delta\gamma/(E^*R) = 4 \times 10^{-5}$. Within the range of parameters considered in our study, the limiting pull-off force does not exceed 1.2 times the solid-sphere result. We now observe that for $\Delta\gamma/(E^*R)$ values ranging from 8×10^{-6} to 1.6×10^{-3}, the pull-off force remains within 0.4 to 1.2 times the solid-sphere result, regardless of the shell thickness. In other words, the pull-off force does not deviate significantly from the solid-sphere pull-off force.

It is worth noting that in the experiments conducted by Zhao et al. (2024), a "sudden augmentation" in the pull-off force was observed as the shell thickness decreased. This phenomenon is consistent with our finding that the pull-off force increases at small thicknesses. In Fig. 6, the experimental results of Zhao et al. are plotted alongside our results in the JKR limit, using the same parameters reported in their study. The "sudden augmentation" is clearly observed for the VPS-32 material, and the corresponding thickness at which this increase occurs is close to the critical thickness show in our results. In contrast, no obvious increase in pull-off force is observed for the VPS-8 material. In this case, the critical thickness is smaller than that of VPS-32, which may explain the absence of augmentation—it likely occurs at a thickness range smaller than those tested in the experiments.

However, we also acknowledge that the experiments by Zhao et al. (2024) exhibited considerable fluctuations and suggest the potential presence of a non-single-minimum form of the pull-off force. Such phenomena may arise from the complex real conditions

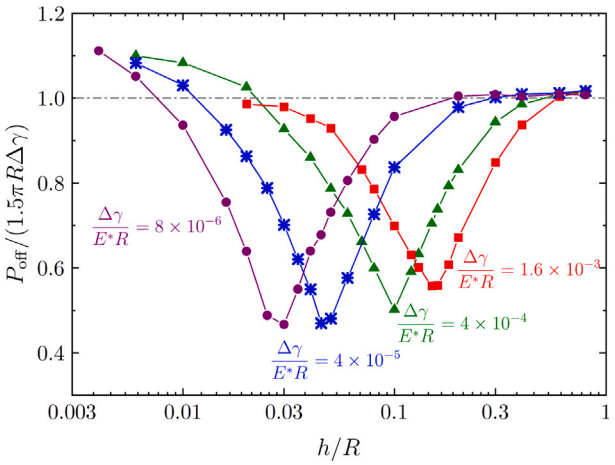

Fig. 5. Normalized pull-off force as a function of thickness for different $\Delta\gamma/(E^*R)$.

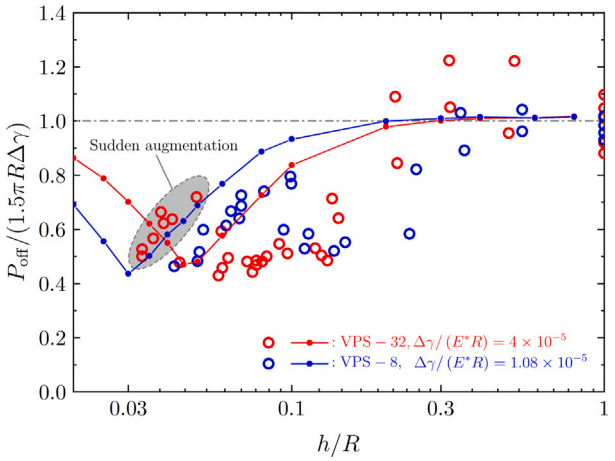

Fig. 6. Comparison between the experimental results of Zhao et al. (2024) (shown as circles) and the results in the JKR limit (shown as curves).

in experiments, such as interfacial friction, surface roughness, or material viscoelasticity. These aspects all warrant further and more in-depth investigation.

In Fig. 7, the critical contact radius at pull-off, denoted as r_c, is shown as a function of shell thickness for different values of $\Delta\gamma/(E^*R)$. As the thickness decreases, a sudden increase in the critical contact radius is observed. This transition occurs at a thickness corresponding to the minimum in the pull-off force. For smaller thicknesses, the increase in pull-off force can be qualitatively explained using Rivlin's peeling theory (Kendall, 1971; Rivlin, 1997). According to this theory, the peeling force scales with the work of adhesion times the perimeter of the contact area, suggesting an approximate pull-off force of $P_{\rm off} \approx \Delta\gamma 2\pi r_c$. In Fig. 8, the pull-off forces are shown alongside $\Delta\gamma 2\pi r_c$ for $\Delta\gamma/(E^*R) = 4\times10^{-4}$ and 1.6×10^{-3}. It is worth noting that the peeling angle introduces a factor greater than one, therefore this estimate underestimates the actual pull-off force. A closed-form theoretical explanation remains an open topic for further investigation.

4. Results account for interfacial traction

The method present in Section 2.3 allows us to simulate the results for finite Tabor parameters. In these results, the pull-off force is defined as the maximum attractive force during unloading. In Fig. 9, we plot the relationship between pull-off force and thickness for different values of $\Delta\gamma/(E^*R)$ at $\mu = 0.2$. For $\mu = 0.2$, the result in the limit of large thickness (where h/R approaches 1) is already close to that of a solid sphere in the DMT limit. It is worth noting that although the method considering interfacial traction includes geometric nonlinearity, we still obtain a figure similar to Fig. 5: increasing $\Delta\gamma/(E^*R)$ leads to a larger critical thickness, while the asymptotic pull-off force at zero thickness becomes smaller. This indicates that for thinner shells, $\Delta\gamma/(E^*R)$ plays a more dominant role in determining the pull-off force-thickness behavior.

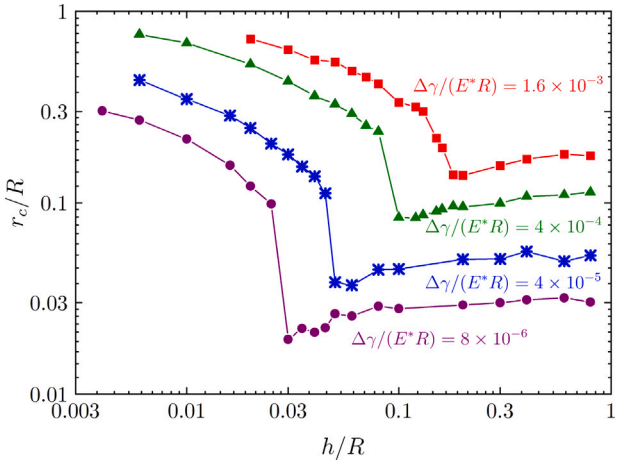

Fig. 7. The contact radius at pull-off as a function of thickness for different $\Delta\gamma/(E^*R)$.

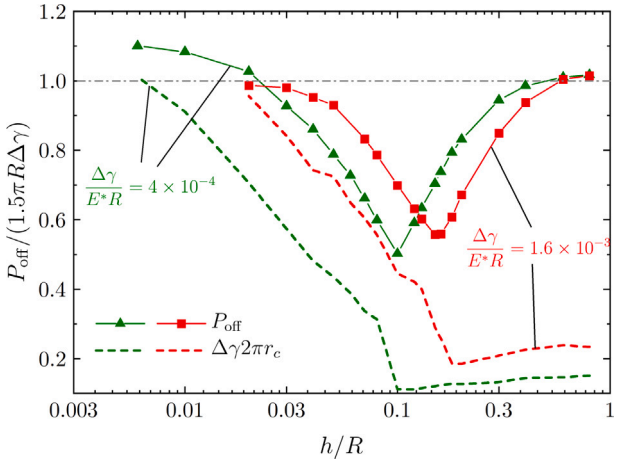

Fig. 8. Comparison of the pull-off force with $\Delta\gamma 2\pi r_c$.

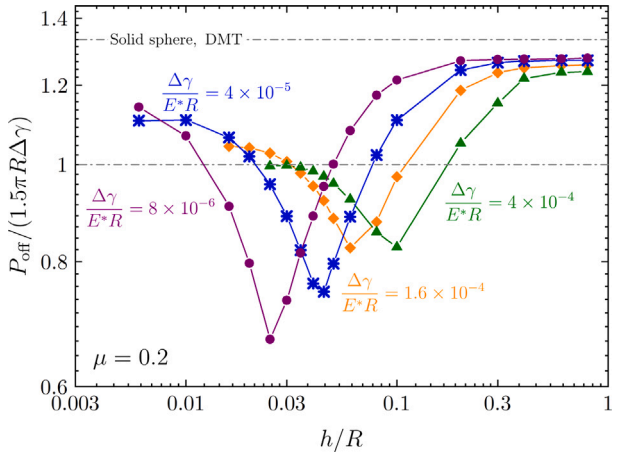

Fig. 9. Normalized pull-off force as a function of thickness for different $\Delta\gamma/(E^*R)$, for $\mu = 0.2$.

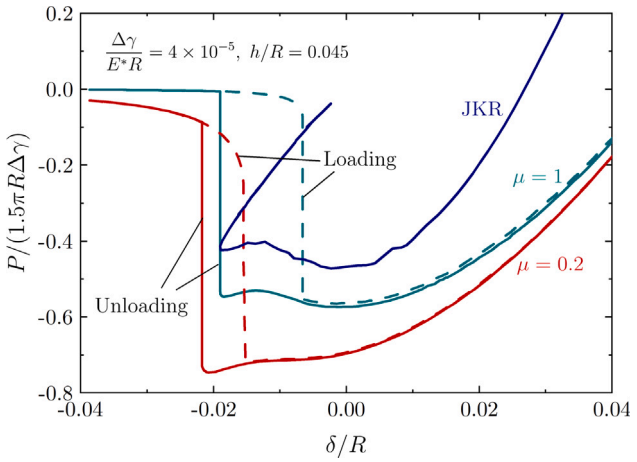

Fig. 10. Comparison of normalized load–displacement curves for different Tabor parameter, including JKR limit.

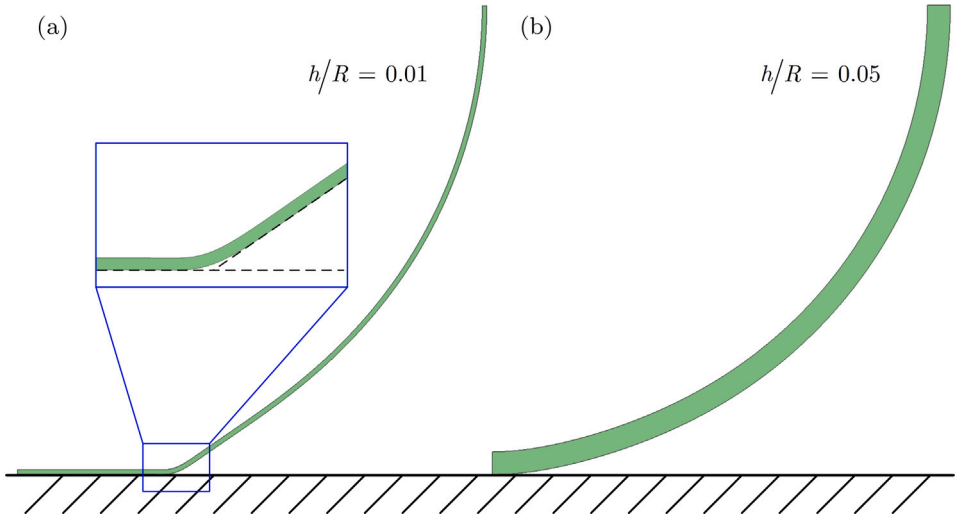

Fig. 11. Deformed states at pull-off for $\mu = 0.2$, $\Delta\gamma/(E^*R) = 4 \times 10^{-5}$, with (a) $h/R = 0.01$ and (b) $h/R = 0.05$.

Figs. 5 and 9 show that, for the same $\Delta\gamma/(E^*R)$, the pull-off force reaches its minimum value at nearly the same thickness. As a example, for $\Delta\gamma/(E^*R) = 4\times10^{-5}$ and $\mu = 0.2$ and 1, the load–displacement curves at the thickness ($h/R = 0.045$) where the pull-off force approaches its minimum are plotted in Fig. 10. The load–displacement curve obtained by the JKR approach is also shown. Through the JKR approach, the difference between loading and unloading cannot be distinguished. In contrast, when the traction law is taken into account, the loading and unloading curves differ. As a result, adhesive hysteresis can be observed in the curves for both $\mu = 1$ and $\mu = 0.2$. It can be observed that the unloading curves more closely resemble the JKR limit. In the unloading curves for both $\mu = 1$ and $\mu = 0.2$, two valleys similar to those in the JKR curve can be observed, and the forces corresponding to these two valleys are nearly identical. As discussed earlier, this explains why the pull-off force exhibits a minimum, which has now been demonstrated by two independent approaches.

Finally, we present the deformed states of the spherical shell at pull-off for $\mu = 0.2$, $\Delta\gamma/(E^*R) = 4\times10^{-5}$, and $h/R = 0.01$ or $h/R = 0.05$, as shown in Fig. 11. For the case of $h/R = 0.01$, the shell undergoes pronounced deformation at pull-off, with a relatively large contact radius; the curvature of the shell immediately outside the contact edge is almost flattened, as illustrated in the inset of Fig. 11(a). In contrast, for $h/R = 0.05$, the deformation at pull-off is much less significant. The contact radius is substantially smaller than in the $h/R = 0.01$ case, and the non-contacting portion of the shell still retains a noticeable curvature.

5. Conclusion

In the present study, we investigate the adhesive contact between an elastic spherical shell and a rigid plane from multiple perspectives. Our main finding is a non-monotonic relationship between the pull-off force and the shell thickness: when the thickness

is greater than a critical value, the pull-off force decreases with decreasing thickness; however, below this critical value, the trend reverses, and the pull-off force increases as the shell becomes thinner. We show that a dimensionless adhesion parameter, $\Delta\gamma/(E^*R)$, has a significant influence on the critical thickness, whereas the Tabor parameter has a negligible effect.

We examined the load–displacement curves and found that the observed non-monotonicity of pull-off force arises from the competition between two local minima on the load–displacement curve. For relatively thick shells, the load–displacement curve exhibits only a single minimum, which corresponds to the pull-off force and decreases as the shell thickness is reduced. As the shell becomes thinner, a second minimum emerges on the curve. The value of this second minimum gradually increases and eventually surpasses that of the first. The critical thickness corresponds to the point at which the two minima yield equal forces. For cases where the thickness is below this critical value, we find that the enhanced pull-off force originates from a sharp increase in the contact area at detachment.

It is worth noting that the JKR approach adopted in Section 2.2 has already been extended to the adhesive contact between a sphere and a hyperelastic half-space (Lin and Chen, 2006) or layer (Lin et al., 2008). Whether this method can be further generalized to the case of a hyperelastic spherical shell also remains an open possibility.

CRediT authorship contribution statement

Shi-Wen Chen: Writing – review & editing, Writing – original draft, Visualization, Software, Methodology, Investigation, Formal analysis, Data curation. **Gang-Feng Wang:** Supervision, Funding acquisition. **Michele Ciavarella:** Writing – review & editing, Supervision, Formal analysis, Data curation, Conceptualization.

Declaration of competing interest

The authors declare that they have no known competing financial interests or personal relationships that could have appeared to influence the work reported in this paper.

Acknowledgments

MC acknowledges support from the Italian Ministry of Education, University and Research (MIUR) under the program “Departments of Excellence” (L.232/2016) and “PRIN 2022” (Project ID: Prot.2022Y78C3K, CUP: D53C24004340006). GFW and SWC acknowledges support from the National Natural Science Foundation of China (Grant No. 12372100).

Data availability

Data will be made available on request.

References

Afferrante, L., et al., 2013. Adhesion of elastic thin films: Double peeling of tapes versus axisymmetric peeling of membranes. Tribol. Lett. 52 (3), 439–447.
Chen, E.R., Dai, Z.H., 2023. Axisymmetric peeling of thin elastic films: A perturbation solution. J. Appl. Mech.-Trans. Asme 90 (10), 101011.
Ciavarella, M., 2018. An approximate JKR solution for a general contact, including rough contacts. J. Mech. Phys. Solids 114, 209–218.
Ciavarella, M., 2022. An upper bound for viscoelastic pull-off of a sphere with a Maugis-Dugdale model. J. Adhes. 98 (13), 2118–2131.
Delcea, M., Möhwald, H., Skirtach, A.G., 2011. Stimuli-responsive LbL capsules and nanoshells for drug delivery. Adv. Drug Deliv. Rev. 63 (9), 730–747.
Derjaguin, B.V., Muller, V.M., Toporov, Y.P., 1975. Effect of contact deformations on adhesion of particles. J. Colloid Interface Sci. 53 (2), 314–326.
Dugdale, D.S., 1960. Yielding of steel sheets containing slits. J. Mech. Phys. Solids 8 (2), 100–104.
Elsner, N., Dubreuil, F., Fery, A., 2004. Tuning of microcapsule adhesion by varying the capsule-wall thickness. Phys. Rev. E 69 (3), 031802.
Fery, A., Weinkamer, R., 2007. Mechanical properties of micro- and nanocapsules: Single-capsule measurements. Polymer 48 (25), 7221–7235.
Greenwood, J.A., 2010. Contact between an axisymmetric indenter and a viscoelastic half-space. Int. J. Mech. Sci. 52 (6), 829–835.
Greenwood, J.A., Johnson, K.L., 1981. The mechanics of adhesion of viscoelastic solids. Philos. Mag. A-Phys. Condens. Matter Struct. Defects Mech. Prop. 43 (3), 697–711.
J.A., Greenwood, 1997. Adhesion of elastic spheres. Proc. R. Soc. A-Math. Phys. Eng. Sci. 453 (1961), 1277–1297.
Johnson, K.L., 1985. Contact Mechanics. Cambridge University Press.
Johnson, K.L., Greenwood, J.A., 1997. An adhesion map for the contact of elastic spheres. J. Colloid Interface Sci. 192 (2), 326–333.
Johnson, K.L., Kendall, K., Roberts, A.D., 1971. Surface energy and contact of elastic solids. Proc. R. Soc. Lond. Ser. A-Math. Phys. Sci. 324 (1558), 301–313.
Kadin, Y., Kligerman, Y., Etsion, I., 2008. Loading-unloading of an elastic–plastic adhesive spherical microcontact. J. Colloid Interface Sci. 321 (1), 242–250.
Kendall, K., 1971. Adhesion and surface energy of elastic solids. J. Phys. D: Appl. Phys. 4 (8), 1186–1195.
Knoche, S., Kierfeld, J., 2014. The secondary buckling transition: Wrinkling of buckled spherical shells. Eur. Phys. J. E 37 (7), 62.
Komura, S., Tamura, K., Kato, T., 2005. Buckling of spherical shells adhering onto a rigid substrate. Eur. Phys. J. E 18 (3), 343–358.
Lin, Y.Y., Chang, C.F., Lee, W.T., 2008. Effects of thickness on the largely-deformed JKR (Johnson-Kendall-Roberts) test of soft elastic layers. Int. J. Solids Struct. 45 (7–8), 2220–2232.
Lin, Y.Y., Chen, H.Y., 2006. Effect of large deformation and material nonlinearity on the JKR (Johnson-Kendall-Roberts) test of soft elastic materials. J. Polym. Sci. Part B-Polym. Phys. 44 (19), 2912–2922.
Longair, M.S., 2020. Theoretical Concepts in Physics: An Alternative View of Theoretical Reasoning in Physics, third ed. Cambridge University Press.
Maugis, D., 1992. Adhesion of spheres: the JKR-DMT transition using a Dugdale model. J. Colloid Interface Sci. 150 (1), 243–269.
Michel, J.P., et al., 2006. Nanoindentation studies of full and empty viral capsids and the effects of capsid protein mutations on elasticity and strength. Proc. Natl. Acad. Sci. USA 103 (16), 6184–6189.
Mu, T., et al., 2025. Nonlinear contact mechanics of soft elastic spheres under extreme compression. J. Mech. Phys. Solids 203, 106229.

Muller, V.M., Yushchenko, V.S., Derjaguin, B.V., 1980. On the influence of molecular forces on the deformation of an elastic sphere and its sticking to a rigid plane. J. Colloid Interface Sci. 77 (1), 91–101.
Pauchard, L., Pomeau, Y., Rica, S., 1997. Deformation of elastic shells. Comptes Rendus L Acad. Sci. Ser. Ii Fasc. B-Mec. Phys. Astron. 324 (7), 411–418.
Pauchard, L., Rica, S., 1998. Contact and compression of elastic spherical shells: the physics of a 'ping-pong' ball. Philos. Mag. B-Phys. Condens. Matter Stat. Mech. Electron. Opt. Magn. Prop. 78 (2), 225–233.
Rivlin, R.S., 1997. In: Barenblatt, G.I., Joseph, D.D. (Eds.), The Effective Work of Adhesion, in Collected Papers of R.S. Rivlin: Volume I and II. Springer New York, New York, NY, pp. 2611–2614.
Sahli, R., et al., 2024. Frictional contact of soft polymeric shells. Phys. Rev. Lett. 133 (10), 106202.
Shen, J.H., et al., 2024. Exploiting interfacial instability during peeling a flexible plate from elastic films. J. Mech. Phys. Solids 192, 105821.
Shi, J.Y., Müftü, S., Wan, K.T., 2011. Adhesion of an elastic convex shell onto a rigid plate. J. Adhes. 87 (6), 579–594.
Shull, K.R., 2002. Contact mechanics and the adhesion of soft solids. Mater. Sci. Eng. R-Rep. 36 (1), 1–45.
Song, Z., Komvopoulos, K., 2011. Adhesion-induced instabilities in elastic and elastic–plastic contacts during single and repetitive normal loading. J. Mech. Phys. Solids 59 (4), 884–897.
Tabor, D., 1977. Surface forces and surface interactions. J. Colloid Interface Sci. 58 (1), 2–13.
Tamura, K., Komura, S., Kato, T., 2004. Adhesion induced buckling of spherical shells. J. Phys.-Condens. Matter 16 (39), L421–L428.
Vallet, D., Barquins, M., 2002. Adhesive contact and kinetics of adherence of a rigid conical punch on an elastic half-space (natural rubber). Int. J. Adhes. Adhes. 22 (1), 41–46.
Vaziri, A., 2009. Mechanics of highly deformed elastic shells. Thin-Walled Struct. 47 (6–7), 692–700.
Yang, F.Q., 2011. Adhesive contact between a rigid axisymmetric indenter and a neo-Hookean solid. J. Adhes. 87 (3), 180–193.
Youssefian, S., Rahbar, N., Torres-Jara, E., 2014. Contact behavior of soft spherical tactile sensors. IEEE Sensors J. 14 (5), 1435–1442.
Yu, C.L., et al., 2024. Stiffer is stickier: Adhesion in elastic nanofilms. Nano Lett. 25 (5), 1876–1882.
Yuan, W.K., et al., 2024. Adhesion of a rigid sphere to a freestanding elastic membrane with pre-tension. J. Appl. Mech.-Trans. Asme 91 (12), 121008.
Zhao, C.X., Wan, K.T., Shan, W.L., 2024. Progressive adhesion mechanics of elastomeric shells against a rigid substrate: From thin to thick. Extrem. Mech. Lett. 68, 102140.
Zhao, C.X., et al., 2022. Adherence of a hyperelastic shell on a rigid planar substrate. Int. J. Solids Struct. 236–237, 111351.
Zhao, C., et al., 2025. Soft shell grippers with highly tunable dry adhesion through low negative pressure for universal manipulation. Adv. Funct. Mater. 2504871.
Zheng, W., Dai, Z., 2025. Universal pull-off force for separating a rigid sphere from a membrane. J. Mech. Phys. Solids 201, 106163.